RCP (3)

J. DOUGLAS - J.E. SANTOS - J.L. HENSLEY - M.E. MORLEY

REND. SEM. MAT.
UNIVERS. POLITECN. TORINO
Fascicolo Speciale (1991)
Numerical Methods

ESTRATTO

SIMULATION OF WAVES ARISING IN ACOUSTIC WELL-LOGGING

LIBRERIA EDITRICE UNIVERSITARIA LEVROTTO & BELLA
CORSO VITTORIO EMANUELE 26/F - TORINO - CORSO LUIGI EINAUDI 57

Rend. Sem. Mat. Univ. Pol. Torino
Fascicolo Speciale 1991
Numerical Methods

J. Douglas - J.E. Santos - J.L. Hensley - M.E. Morley

SIMULATION OF WAVES ARISING IN ACOUSTIC WELL-LOGGING

Abstract. *Waves arising in acoustic well-logging associated with Biot media are approximated by efficient finite element methods. Several numerical experiments are reported.*

§1. Introduction

In this paper we are concerned with the numerical simulation of waves arising in acoustic well-logging. The problem consists of acoustic and elastic wave propagation in a cylindrical, fluid-filled borehole Ω_f surrounded by a fluid-saturated porous solid Ω_p. Compressional point sources are excited at points on the centerline (and z-axis) $\mathcal{L}$ of the borehole, and the pressure is recorded by receivers also located along $\mathcal{L}$, as well as various displacements at points in the porous medium. For simplicity we assume the whole system $\Omega = \Omega_f \cup \Omega_p$ is isotropic and radially symmetric about $\mathcal{L}$. The acoustic wave equation for compressible, inviscid fluids is used to describe the propagation of waves in Ω_f. Biot's equations [2], [3] are used to describe the propagation of waves in the porous medium Ω_p. Absorbing boundary conditions are used on the artificial boundaries used to limit the domain [8], [12]. On the surface between Ω_f and Ω_p we have used the boundary condition suggested in [11],

The research of Douglas and Morley was supported in part by the National Science Foundation, that of Santos by CONICET and the U.S. Army, and that of Hensley by the U.S. Army.

which represents a way of including the effects of the mud cake on the wave field; in the experiments reported in §3 we used the special case for a closed interface.

Finite element methods for approximating the solution to this problem were introduced and analyzed in an earlier paper [12]. In this paper we show numerical results obtained by the implementation of this technique. We compare the resulting waves when the porous medium consists of sandstone saturated by different fluids.

The organization of this paper is as follows. The model and the finite element technique are described in §2. The numerical experiments are described in §3.

§2. The model

As announced above, we shall consider the propagation of waves in the isotropic and radially symmetric domain $\Omega = \Omega_f \cup \Omega_p$. We use the natural cylindrical coordinates. Without loss of generality the system can be described as follows:

$$\begin{aligned}
\Omega &= \{(r,\theta,z): \ 0 \le r \le R_p\,,\ 0 \le \theta \le 2\pi\,,\ 0 \le z \le z_B\}\,,\\
\Omega_f &= \{(r,\theta,z): \ 0 \le r \le R_f\,,\ 0 \le \theta \le 2\pi\,,\ 0 \le z \le z_B\}\,,\\
\Omega_p &= \{(r,\theta,z): \ R_f \le r \le R_p\,,\ 0 \le \theta \le 2\pi\,,\ 0 \le z \le z_B\}\,.
\end{aligned}$$

Let the artificial top and bottom boundaries of Ω_f be labeled Γ_1, the artificial top and bottom boundaries of Ω_p be labeled Γ_{21}, the artificial outer boundary of Ω_p be labeled Γ_{22}, and let the boundary between Ω_p and Ω_f be Γ_3. A vertical cross section for any $\theta = \theta_0$ is shown in Figure 1.

Let $u_1 = (u_{1r}, 0, u_{1z})$ represent the fluid displacement in the borehole and let $u_2 = (u_{2r}, 0, u_{2z})$ and $\underset{\sim}{u}_3 = (\underset{\sim}{u}_{3r}, 0, \underset{\sim}{u}_{3z})$ be the vectors representing, respectively, the solid and the averaged fluid displacements in the porous medium. Set $u_3 = \phi(r,z)(\underset{\sim}{u}_3 - u_2)$, where $\phi(r,z)$ is the effective porosity. Then, using the symmetry, the components of the strain tensor $\varepsilon(u_2)$ in the solid part of Ω_p can be written as follows [7] [6]:

$$\varepsilon_{rr}(u_2) = \frac{\partial u_{2r}}{\partial r}$$

$$\varepsilon_{rz}(u_2) = \frac{1}{2}\left(\right.$$

$$\varepsilon_{r\theta}(u_2) = \frac{1}{2}\left(\right.$$

$$\varepsilon_{\theta z}(u_2) = \frac{1}{2}\left(\right.$$

Also,

$$\nabla \cdot u_2 = \varepsilon$$

Denote the total st
by $p(u_2, u_3)$. The stress-

$$\tau_{rr}(u_2, u$$

$$\tau_{\theta\theta}(u_2, u$$

$$\tau_{zz}(u_2, u$$

$$\tau_{rz}(u$$

$$\tau$$

$$p(u_2, u$$

In the above expressions

$$\varepsilon_{rr}(u_2) = \frac{\partial u_{2r}}{\partial r} \ , \quad \varepsilon_{\theta\theta}(u_2) = \frac{u_{2r}}{r} \ , \quad \varepsilon_{zz}(u_2) = \frac{\partial u_{2z}}{\partial z} \ ,$$

$$\varepsilon_{rz}(u_2) = \frac{1}{2}\left(\frac{\partial u_{2r}}{\partial z} + \frac{\partial u_{2z}}{\partial r}\right) \ ,$$

$$\varepsilon_{r\theta}(u_2) = \frac{1}{2}\left(\frac{1}{r}\frac{\partial u_{2r}}{\partial \theta} + \frac{\partial u_{2\theta}}{\partial r} - \frac{u_{2\theta}}{r}\right) = 0 \ ,$$

$$\varepsilon_{\theta z}(u_2) = \frac{1}{2}\left(\frac{\partial u_{2\theta}}{\partial z} + \frac{1}{r}\frac{\partial u_{2z}}{\partial \theta}\right) = 0 \ .$$

Also,

$$\nabla \cdot u_2 = \varepsilon_{rr} + \varepsilon_{\theta\theta} + \varepsilon_{zz} = \frac{1}{r}\frac{\partial (r u_{2r})}{\partial r} + \frac{\partial u_{2z}}{\partial z} \ .$$

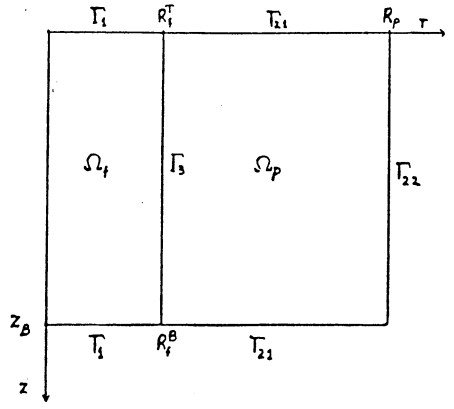

Figure 1

Denote the total stress tensor by $\tau(u_2, u_3)$ and the fluid pressure in Ω_p by $p(u_2, u_3)$. The stress-strain relations can then be written as follows [2]:

$$\begin{aligned}
\tau_{rr}(u_2, u_3) &= A\nabla \cdot u_2 + 2N\,\varepsilon_{rr}(u_2) + Q\nabla \cdot u_3 \ , \\
\tau_{\theta\theta}(u_2, u_3) &= A\nabla \cdot u_2 + 2N\,\varepsilon_{\theta\theta}(u_2) + Q\nabla \cdot u_3 \ , \\
\tau_{zz}(u_2, u_3) &= A\nabla \cdot u_2 + 2N\,\varepsilon_{zz}(u_2) + Q\nabla \cdot u_3 \ , \\
\tau_{rz}(u_2) &= 2N\,\varepsilon_{rz}(u_2) \ , \\
\tau_{r\theta} &= \tau_{\theta z} = 0 \ , \\
p(u_2, u_3) &= -Q\nabla \cdot u_2 - H\nabla \cdot u_3 \ .
\end{aligned} \tag{2.1}$$

In the above expressions $A, N, Q,$ and H are assumed to be functions of r

and z alone. They are also assumed to satisfy the following assumptions:

$$N(r,z) > 0 \ , \quad H(r,z) > 0 \ , \quad \left(A + \frac{2}{3}N\right)(r,z) > 0 \ ,$$
$$\left(A + \frac{2}{3}N - \frac{Q^2}{H}\right)(r,z) > 0 \ , \quad (r,\theta,z) \in \overline{\Omega}_p = \Omega_p \cup \partial\Omega_p \ . \tag{2.2}$$

These assumptions are necessary for the strain energy density to be positive. Next, let $\rho = \rho(r,z)$ be the total mass density of the bulk material in Ω_p and let $\rho_f = \rho_f(r,z)$ be the mass density of fluid both in Ω_f and in Ω_p. Also, let $g = g(r,z)$ be the mass coupling parameter between the fluid and the solid in Ω_p [3]. Assume that

$$\rho g(r,z) - \rho_f^2(r,z) > 0 \ , \qquad (r,\theta,z) \in \overline{\Omega}_p \ ; \tag{2.3}$$

this is a necessary and sufficient condition for the kinetic energy density in Ω_p to be positive. Let $\mu = \mu(r,z)$ represent the fluid viscosity, $K = K(r,z)$ the scalar rock permeability, and $A_f = A_f(r,z)$ the incompressibility modulus of the fluid in Ω_f. The three functions $\mu, K,$ and A_f are assumed to be bounded above and below by positive constants.

Let initial conditions $u_1^0(r,z) = (u_{1r}^0, 0, u_{1z}^0)$ and $(\partial u_1/\partial t)^0 = v_1^0 = (v_{1r}^0, 0, v_{1z}^0)$ and forces $f_1(r,z,t) = (f_{1r}, 0, f_{1z})$ be given for $(r,\theta,z) \in \Omega_f$. Initial conditions and forces are assumed to be zero in Ω_p. Then the problem can be stated as follows. We want to find $u(r,z,t) = (u_1, u_2, u_3)$, $t \in J = (0,T)$, such that

$$i) \quad \rho_f \frac{\partial^2 u_{1r}}{\partial t^2} - \frac{\partial}{\partial r}(A_f \nabla \cdot u_1) = f_{1r}(r,z,t) \ ,$$

$$ii) \quad \rho_f \frac{\partial^2 u_{1z}}{\partial t^2} - \frac{\partial}{\partial z}(A_f \nabla \cdot u_1) = f_{1z}(r,z,t) \ , \quad \text{for } (r,\theta,z,t) \in \Omega_f \times J \ ,$$

and

$$iii) \quad \rho \frac{\partial^2 u_{2r}}{\partial t^2} + \rho_f \frac{\partial^2 u_{3r}}{\partial t^2} - \frac{1}{r}\frac{\partial}{\partial r}(r\tau_{rr}(u_2,u_3)) - \frac{\partial}{\partial z}\tau_{rz}(u_2) + \frac{\tau_{\theta\theta}(u_2,u_3)}{r} = 0 \ ,$$

$$iv) \quad \rho \frac{\partial^2 u_{2z}}{\partial t^2} + \rho_f \frac{\partial^2 u_{3z}}{\partial t^2} - \frac{1}{r}\frac{\partial}{\partial r} r\tau_{rz}(u_2) - \frac{\partial}{\partial z}\tau_{zz}(u_2,u_3) = 0 \ ,$$

$$v) \quad \rho_f \frac{\partial^2 u_{2r}}{\partial t^2} + g \frac{\partial^2 u_{3r}}{\partial t^2} + \frac{\mu}{K}\frac{\partial u_{3r}}{\partial t} + \frac{\partial}{\partial r} p(u_2,u_3) = 0 \ ,$$

$$vi) \quad \rho_f \frac{\partial^2 u_{2r}}{\partial t^2} + g \frac{\partial^2 u_{3z}}{\partial t^2} + \frac{\mu}{K}\frac{\partial u_{3z}}{\partial t} + \frac{\partial}{\partial z} p(u_2,u_3) = 0 \ , \quad \text{for } (r,\theta,z) \in \Omega_p \times J \ ,$$

subject to the boundary

$$i) \quad -A_f \nabla \cdot u_1$$

$$ii) \quad (-\tau\nu_p \cdot \nu_p \ ,$$
$$B\left(\frac{\partial u}{\partial}\right.$$

$$iii) \quad \tau\nu_p + A_f \nabla$$

$$iv) \quad (u_2 + u_3) \cdot$$

$$v) \quad -p + m\frac{\partial}{\partial}$$

and the initial condition

$$i) \quad u$$

$$ii) \quad ($$

$$iii) \quad \frac{\partial}{\partial}$$

$$iv) \quad \frac{\partial}{\partial}$$

In the above $\nu_i = (\nu_i$ outward normal along vectors along $\partial\Omega_p$.

Equations (2.4)(i pressible, inviscid fluids the fluid-saturated por (2.5)(i-ii) are artificial that waves arriving nor tely (i.e., passed throug the second, (2.5ii), is d a symmetric and positi sical parameters $A, N,$ [12]. The third boundar stresses and requires th (2.5iv) imposes continu boundary conditions, (on both sides of Γ_3.

subject to the boundary conditions

$$
\begin{aligned}
&i) \quad -A_f \nabla \cdot u_1 = \sqrt{\rho_f A_f}\, \frac{\partial u_1}{\partial t} \cdot \nu_f \ , \quad (r,\theta,z,t) \in \Gamma_1 \times J \ , \\
&ii) \quad (-\tau \nu_p \cdot \nu_p \ , \ -\tau \nu_p \cdot \chi_p^1 \ , \ -\tau \nu_p \cdot \chi_p^2 \ , \ p)^t = \\
&\qquad B \left(\frac{\partial u_2}{\partial t} \cdot \nu_p \ , \ \frac{\partial u_2}{\partial t} \cdot \chi_p^1 \ , \ \frac{\partial u_2}{\partial t} \cdot \chi_p^2 \ , \ \frac{\partial u_3}{\partial t} \cdot \nu_p \right)^t \ , \\
&\qquad\qquad (r,\theta,z,t) \in (\Gamma_{21} \cup \Gamma_{22}) \times J = \Gamma_2 \times J \ , \\
&iii) \quad \tau \nu_p + A_f \nabla \cdot u_1 \nu_f = 0 \ , \qquad (r,\theta,z,t) \in \Gamma_3 \times J \ , \\
&iv) \quad (u_2 + u_3) \cdot \nu_p + u_1 \cdot \nu_f = 0 \ , \qquad (r,\theta,z,t) \in \Gamma_3 \times J \ , \\
&v) \quad -p + m \frac{\partial u_3}{\partial t} \cdot \nu_p = A_f \nabla \cdot u_1 \ , \quad (r,\theta,z,t) \in \Gamma_3 \times J \ ,
\end{aligned}
\tag{2.5}
$$

and the initial conditions

$$
\begin{aligned}
&i) \quad u_1(r,z,0) = u_1^0(r,z) \ , \qquad (r,\theta,z) \in \Omega_f \ , \\
&ii) \quad (u_2,u_3)(r,z,0) = 0 \ , \qquad (r,\theta,z) \in \Omega_p \ , \\
&iii) \quad \frac{\partial u_1}{\partial t}(r,z,0) = v_1^0(r,z) \ , \qquad (r,\theta,z) \in \Omega_f \ , \\
&iv) \quad \frac{\partial}{\partial t}(u_2,u_3)(r,z,0) = 0 \ , \qquad (r,\theta,z) \in \Omega_p \ .
\end{aligned}
\tag{2.6}
$$

In the above $\nu_i = (\nu_{ir}, \nu_{i\theta}, \nu_{iz}) = (\nu_{ir}, 0, \nu_{iz})$, $i = f,p$, denotes the unit outward normal along $\partial\Omega_i$ and χ_p^1 and χ_p^2 denote orthogonal unit tangent vectors along $\partial\Omega_p$.

Equations (2.4)(i)-(ii) are the standard equations of motion for compressible, inviscid fluids. The equations (2.4)(iii)-(vi) are Biot's equations for the fluid-saturated porous medium Ω_p [2], [3]. The boundary conditions (2.5)(i-ii) are artificial boundary conditions. They are derived by requiring that waves arriving normally to an artificial boundary be absorbed completely (i.e., passed through transparently). The first, (2.5i), is well known, and the second, (2.5ii), is derived in [12]. The matrix $B(r,t) \in R^{4\times4}$ in (2.5ii) is a symmetric and positive-definite matrix whose terms depend upon the physical parameters A, N, Q, H, ρ, ρ_f, and g. The exact form of B is given in [12]. The third boundary condition, (2.5iii), imposes continuity on the normal stresses and requires the vanishing of the tangential stresses along Γ_3, and (2.5iv) imposes continuity on the normal displacement along Γ_3. The last boundary conditions, (2.5v), was suggested in [11] to relate the fluid pressure on both sides of Γ_3. The nonnegative coefficient $m = m(z)$ is used to

describe the behavior of the mudcake; it represents a surface impedance. In the numerical experiments we choose the limit case $m = +\infty$, corresponding to a closed interface, which in most cases is a good approximation to the real conditions inside the borehole. Thus, (2.5v) is replaced by

$$u_3 \cdot \nu = 0 \ , \quad \text{on} \ \ \Gamma_3 \times J \ ,$$

and (2.5iv) reduces to

$$u_2 \cdot \nu_p + u_1 \cdot \nu_f = 0 \quad \text{on} \ \ \Gamma_3 \times J \ .$$

Existence and uniqueness results for the above system were stated and proved in [12]. Also, in the same paper, a finite element procedure for obtaining an approximate solution was defined and analyzed. We summarize this procedure below.

Let $\widetilde{H}(div, \Omega_i)$, $i = f, p$, be the closed subspace of $H(div, \Omega_i)$ given by

$$\widetilde{H}(div, \Omega_i) = \{\varphi = (\varphi_r, \varphi_\theta, \varphi_z) \in H(div, \Omega_i) \ , \ \varphi_\theta = 0\} \ .$$

Similarly, let

$$\widetilde{H}^1(\Omega_p)^3 = \left\{\varphi = (\varphi_r, \varphi_\theta, \varphi_z) \in H^1(\Omega_p)^3 : \varphi_\theta = 0 \ , \ \frac{\partial \varphi_r}{\partial \theta} = \frac{\partial \varphi_z}{\partial \theta} = 0\right\} \ ;$$

$\widetilde{H}^1(\Omega_p)^3$ is clearly a closed subspace of $H^1(\Omega_p)^3$. Next, let $\widetilde{V} = \widetilde{H}(div, \Omega_f) \times \widetilde{H}^1(\Omega_p)^3 \times \widetilde{H}(div, \Omega_p)$, which is a separable Hilbert space under the natural norm. Since the boundary condition (2.5iv) is an essential boundary condition, it must be imposed on the test space. Hence, we need to restrict the admissible test functions to the set $V = \{(v_1, v_2, v_3) \in \widetilde{V} : (v_2 + v_3 - v_1) \cdot \nu_f = 0 \text{ on } \Gamma_3\}$; V is a closed subspace of $\widetilde{V}$.

The weak form of the problem is found as usual by multiplying the equations (2.4) by admissible test functions and then integrating by parts. The resulting equation is

$$\left(\rho_f \frac{\partial^2 u_1}{\partial t^2} \ , \ v_1\right)_f + \left(\mathcal{A} \frac{\partial^2 (u_2, u_3)}{\partial t^2} \ , \ (v_2, v_3)\right)_p + \left(\mathcal{C} \frac{\partial (u_2, u_3)}{\partial t} \ , \ (v_2, v_3)\right)_p$$
$$+ \Lambda(u, v) + \langle \sqrt{\rho_f A_f} \frac{\partial u_1}{\partial t} \cdot \nu_f \ , \ v_1 \cdot \nu_f \rangle_{\Gamma_1} + \langle m \frac{\partial u_3}{\partial t} \cdot \nu_p \ , \ v_3 \cdot \nu_p \rangle_{\Gamma_3}$$
$$+ \langle B \left(\frac{\partial u_2}{\partial t} \cdot \nu_p \ , \ \frac{\partial u_2}{\partial t} \cdot \chi_p^1 \ , \ \frac{\partial u_2}{\partial t} \cdot \chi_p^2 \ , \ \frac{\partial u_3}{\partial t} \cdot \nu_p\right)^t \ , \ (v_2 \cdot \nu_p \ , \ v_2 \cdot \chi_p^1 \ , \ v_2 \cdot \chi_p^2 \ , \ v_3 \cdot \nu_p)^t \rangle_{\Gamma_2}$$
$$= (f_1, v_1)_f \ , \quad v = (v_1, v_2, v_3) \in V \ , \ \ t \in J \ .$$

In the above equation $\mathcal{A}(r,z)$ and $\mathcal{C}(r,z)$ are matrices in $R^{4\times 4}$ and are given by

$$\mathcal{A} = \begin{bmatrix} \rho\, I & \rho_f\, I \\ \rho_f\, I & g\, I \end{bmatrix}, \quad \mathcal{C} = \mu K^{-1} \begin{bmatrix} 0 & 0 \\ 0 & I \end{bmatrix},$$

where I is the identity matrix in $R^{2\times 2}$, $\mathcal{C}$ is nonnegative, and $\mathcal{A}$ is positive definite. Also, $\Lambda(v,w)$ is the symmetric, bilinear form defined on $\widetilde{V}$ by

$$\begin{aligned}\Lambda(v,w) = {} & (A_f \nabla\cdot v_1\,,\ \nabla\cdot w_1)_f + (\tau_{rr}(v_2,v_3)\,,\ \varepsilon_{rr}(w_2))_p \\ & + (\tau_{\theta\theta}(v_2,v_3)\,,\ \varepsilon_{\theta\theta}(w_2))_p + (\tau_{zz}(v_2,v_3)\,,\ \varepsilon_{zz}(w_2))_p \\ & + 2(\tau_{rz}(v_2,v_3)\,,\ \varepsilon_{rz}(w_2))_p - (p(v_2,v_3)\,,\ \nabla\cdot w_3)_p\,.\end{aligned}$$

As a result of Korn's second inequality and the physical assumptions on the coefficients, it can be shown [12] that

$$\Lambda(v,v) \geq c_1 \|v\|^2_{\widetilde{V}} - c_2(\|v_1\|^2_{0,\Omega_f} + \|(v_2,v_3)\|^2_{0,\Omega_p}), \quad v \in \widetilde{V}\,.$$

The finite element procedure can then be formulated as follows. For $0 < h < 1$, let $\tau_h^f = \tau_h^f(\Omega_f)$ and $\tau_h^p = \tau_h^p(\Omega_p)$ be quasiregular partitions of Ω_f and Ω_p into elements generated by rotating rectangles in r and z about the z-axis. Let the rectangles be bounded in diameter by h. Let $P_{1,1}(r,z)$ denote the piecewise bilinear polynomial functions in r and z, and set

$$M_h = \{\varphi = (\varphi_r,\, 0,\, \varphi_z) \in C^0(\overline{\Omega}_p) : \varphi_r \in rP_{1,1}(r,z) \text{ and } \varphi_z \in P_{1,1}(r,z)\}\,.$$

Clearly, $M_h \subset \widetilde{H}^1(\Omega_p)^3$. The r component is multiplied by r in order to ensure that all the terms of $\varepsilon(\varphi)$ remain piecewise polynomials. The approximation property

$$\inf_{\varphi\in M_h} \{\|v-\varphi\|_{0,\Omega_p} + h\,\|v-\varphi\|_{1,\Omega_p}\} \leq ch^s \|v\|_{s,\Omega_p}\,, \quad s = 1,2, \tag{2.8}$$

holds; this result is proved in [9].

Let $W_h(\Omega_i)$, $i = f, p$, be the vector part of the lowest order mixed finite element space defined by one of the authors in [9]. Away from $r = 0$, the elements in $W_h(\Omega_i)$ are locally of the form $(ar^{-1} + br\,,\ 0\,,\ c + dz)$, while the innermost elements near $r = 0$ have the local form $(br\,,\ 0\,,\ c + dz)$. These have the same approximation properties as the usual zero order mixed finite element spaces [9]:

$$\begin{aligned} &i) \quad \inf_{\varphi\in W_h(\Omega_i)} \|v-\varphi\|_{H(div,\Omega_i)} \leq ch(\|v\|_{1,\Omega_i} + \|\nabla\cdot v\|_{1,\Omega_i})\,, \\ &ii) \quad \inf_{\varphi\in W_h(\Omega_i)} \|v-\varphi\|_{0,\Omega_i} \leq ch\|v\|_{1,\Omega_i}\,. \end{aligned} \tag{2.9}$$

Let $\tilde{V}_h = W_h(\Omega_f) \times M_h \times W_h(\Omega_p)$ and set $V_h = \{v \in \tilde{V}_h : (v_2 + v_3 - v_1) \cdot \nu_f = 0 \text{ on } \Gamma_3\}$. Then $V_h \subset V$ and it follows from (2.8) and (2.9) that

$$\inf_{\varphi \in V_h} [\|v_1 - \varphi_1\|_{0,\Omega_f} + \|(v_2, v_3) - (\varphi_2, \varphi_3)\|_{0,\Omega_f}] \leq ch[\|v_1\|_{1,\Omega_f} + \|(v_2, v_3)\|_{1,\Omega_p}] , \tag{2.10}$$

for $v \in (\tilde{H}^1(\Omega_f)^3 \times \tilde{H}^1(\Omega_p)^3 \times \tilde{H}^1(\Omega_p^3)) \cap V$, and that

$$\inf_{\varphi \in V_h} \|v - \varphi\|_V \leq ch[\|v_1\|_{1,\Omega_f} + \|\nabla \cdot v_1\|_{1,\Omega_f} + \|v_2\|_{2,\Omega_p} + \|v_3\|_{1,\Omega_p} + \|\nabla \cdot v_3\|_{1,\Omega_p}] , \tag{2.11}$$

for $v \in (\tilde{H}(\Omega_p)^3 \times \tilde{H}^2(\Omega_p)^3 \times \tilde{H}^1(\Omega_p)) \cap V$ such that $\nabla \cdot v_1 \in H^1(\Omega_f)$ and $\nabla \cdot v_3 \in H^1(\Omega_p)$.

Let L be a positive integer, $\Delta t = T/L$, and $U^n = U(n\,\Delta t)$. Set

$$d_t U^n = (U^{n+1} - U^n)/\Delta t ,$$
$$\partial U^n = (U^{n+1} - U^{n-1})/(2\,\Delta t) ,$$
$$\partial^2 U^n = (U^{n+1} - 2U^n + U^{n-1})/(\Delta t)^2 .$$

Mass lumping will be used for all terms involving differentiation with respect to time in order to get an explicit procedure. This is equivalent to computing all integrals involving time derivatives using the quadrature rule

$$\int_Q f(r,z)\, r\, dr\, d\theta\, dz \approx \frac{2\pi}{4} h_r h_z [f_1 r_1 + f_2 r_2 + f_3 r_3 + f_4 r_4] , \tag{2.12}$$

where f_i denotes the value of f at the node a_i in the rectangle Q (see Figure 2). Note that the rule (2.12) is exact if $rf(r,z)$ is bilinear.

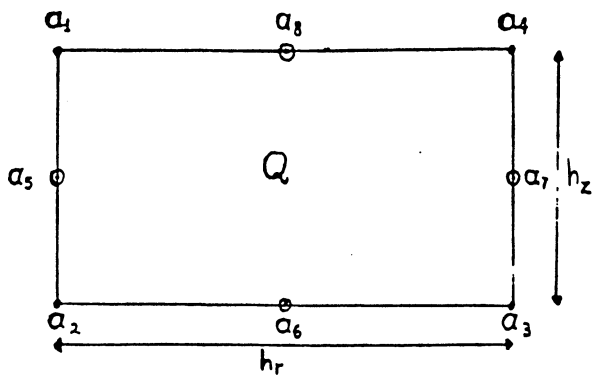

Figure 2

Let $[v,w]_i$ and $|||v|||_i$
$(v,w)_i$ and the norm $\|v\|_i$
rule (2.12). Also let $\langle\langle v,$
using (2.12).

The discrete-time ex
V_h, $n \in \{0,1,...,L\}$, such t

$$[\rho_f \partial^2 U_1^n, v_1]_f + [A\partial^2(U_2, U$$
$$+ \langle\langle \sqrt{\rho_f A_f}\, \partial U_1^n \cdot \nu_f , v_1 \cdot$$
$$+ \langle\langle B(\partial U_2^n \cdot \nu_p , \partial U_2^n \cdot \chi_p^1 ,$$
$$= (f_1^n, v_1)_f , \quad v \in V_h , \quad 1 \leq$$

A stability criterion $\Delta t \leq$
method. An upper boun
is satisfied, and if v^0 an
optimal order estimate hc

$$\max_{1 \leq N \leq L-1} (|||d_t(u_1 - U_1)^N$$

§3. Numerical experin

The finite element
being taken to be rotati
the tests the fluid in the
sound velocity 1250 m/s
be $\rho_f S/\phi$, where S is a
values for S between 2.
The density of the bulk

The main frequency of t
more or less standard in
was chosen to be Berea
data for the formation w
a more effective logging,

Let $[v,w]_i$ and $|||v|||_{0,\Omega_i}$, $i=f,p$, denote, respectively, the inner product $(v,w)_i$ and the norm $\|v\|_{0,\Omega_i}$ computed approximately using the quadrature rule (2.12). Also let $\langle\langle v,w\rangle\rangle$ denote the inner product $\langle v,w\rangle_\Gamma$ computed using (2.12).

The discrete-time explicit Galerkin procedure consists of finding $U^n \in V_h$, $n \in \{0,1,...,L\}$, such that

$$\begin{aligned}&[\rho_f \partial^2 U_1^n, v_1]_f + [\mathcal{A}\partial^2 (U_2,U_3)^n, (v_2,v_3)]_p + [\mathcal{C}\partial (U_2,U_3)^n, (v_2,v_3)]_p + \Lambda(U^n,v)\\ &+ \langle\langle \sqrt{\rho_f A_f}\, \partial U_1^n \cdot \nu_f,\ v_1\cdot\nu_f\rangle\rangle_{\Gamma_1} + \langle\langle m\,\partial U_3^n\cdot\nu_p,\ v_3\cdot\nu_p\rangle\rangle_{\Gamma_3}\\ &+ \langle\langle B(\partial U_2^n\cdot\nu_p, \partial U_2^n\cdot\chi_p^1, \partial U_2^n\cdot\chi_p^2, \partial U_3^n\cdot\nu_p)^t, (v_2\cdot\nu_p, v_2\cdot\chi_p^1, v_2\cdot\chi_p^2, v_3\cdot\nu_p)^t\rangle\rangle_{\Gamma_2}\\ &= (f_1^n, v_1)_f,\quad v\in V_h,\quad 1\le n\le L-1\,.\end{aligned} \tag{2.13}$$

A stability criterion $\Delta t \le c_1 h$ is necessary because of explicit nature of the method. An upper bound for c_1 is given in [12]. If the stability criterion is satisfied, and if v^0 and v^1 are chosen correctly, then [12] the following optimal order estimate holds:

$$\begin{aligned}\max_{1\le N\le L-1}&(|||d_t(u_1-U_1)^N|||_{0,\Omega_p} + |||d_t(u_2-U_2,\,u_3-U_3)^N|||_{0,\Omega_p} + \|u-U)^N\|_V)\\ &\le c(u^0,v^0,u)[(\Delta t)^2 + h]\,.\end{aligned} \tag{2.14}$$

§3. Numerical experiments

The finite element procedure (2.13) was implemented with τ_h^f and τ_h^p being taken to be rotations of uniform rectangles in r and z. For all the tests the fluid in the borehole was taken to have density 1.4 gr/cm^3 and sound velocity 1250 m/sec. The mass-coupling parameter g was chosen to be $\rho_f S/\phi$, where S is a structure parameter. Several authors have reported values for S between 2.1 and 3.3, [5], [10]. Here, we have chosen $S = 2.8$. The density of the bulk material can be obtained by the formula

$$\rho = (1-\phi)\,\rho_s + \phi\rho_f\,.$$

The main frequency of the source was taken to be 21 khz; this frequency is more or less standard in acoustic well-logging field tests. The porous material was chosen to be Berea sandstone saturated by gas or water. The physical data for the formation was taken from [11] and is summarized in Table 1. For a more effective logging, it is desirable that the energy coming from the well

into the formation hit the interface Γ_3 at an angle of approximately 30°. This can be achieved by using two compressional point sources located at the centerline of the borehole, at a distance of one wavelength and fixed with a time delay t_d related to the main frequency and wavelength by the formula

$$t_d \cong .36/\text{main frequency}.$$

The compressional point sources have the form

$$f_1(r,z,t) = g(t)\,\nabla\delta_{r=0,z=z_i}\,, \qquad i=1,2,$$

where $g(t)$ is any desired waveform. We chose [13]

$$g(t) = -2\xi(t-t_s)\,e^{-\xi(t-t_s)^2}\,,$$

with ξ being related to the main frequency chosen. The domain Ω was taken to be 260 cm deep and to have a total radius of 24 cm. The borehole radius above was 8 cm. The tests were run for 2.07 msec with a time step of .0007 msec. Both Δr and Δz we take to be .4 cm. As it is known [2], [3], there are three different kinds of body waves that can propagate in a fluid-saturated porous solid, which we will refer in the text as type I and type II compressional waves and shear waves. Also, we have the direct compressional wave travelling in the fluid in the borehole, and several other types of waves such as the pseudo-Raleigh and Stoneley waves, which are surface-like waves generated by the interaction of Ω_f and Ω_p along Γ_3.

In acoustic well logging a set of receivers is located along the centerline of the borehole at a certain distance from the sources. The numerical experiments locate the sources at depths .22079 m and .27921 m and 6 receivers at increments of .2 m between 1.4 m and 2.4 m below the sources. The deeper source was fired .017 msec after the upper source.

In Figure 3 we show the snapshot of the pressure in the well and the trace of the total stress in the formation (i.e., $\tau_{rr}+\tau_{\theta\theta}+\tau_{zz}$) at time .1 msec. The effect of constructive interference of the wavefronts generated by the point sources in the well is clearly appreciated. We also see the compressional wavefront generated in the formation starting to travel downward with the energy concentrated near the interface.

Figure 4 displays the same quantities as Figure 3 but at times .1 msec and .2 msec to show the evolution of the compressional wavefronts. At time .2 msec we see a better developed wavefront travelling downward in the formation at a much greater speed than the corresponding wavefront in the borehole. The energy radiated back from the formation into the well at the bottom of the snapshot cannot be seen because of its low amplitude compared with the events above in the well.

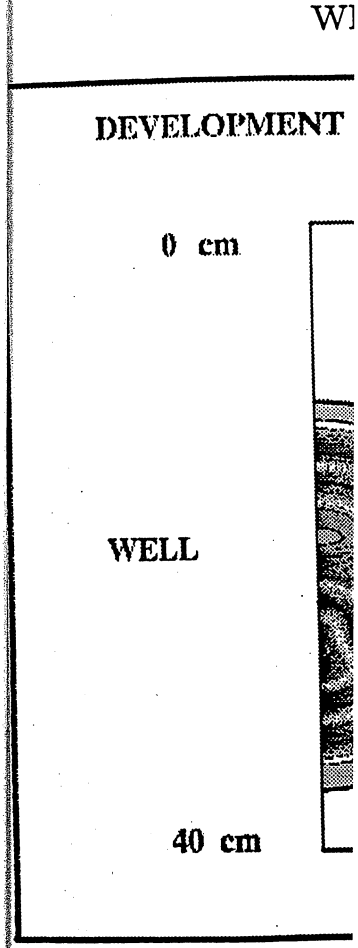

WELL–LOGGING EXAMPLE

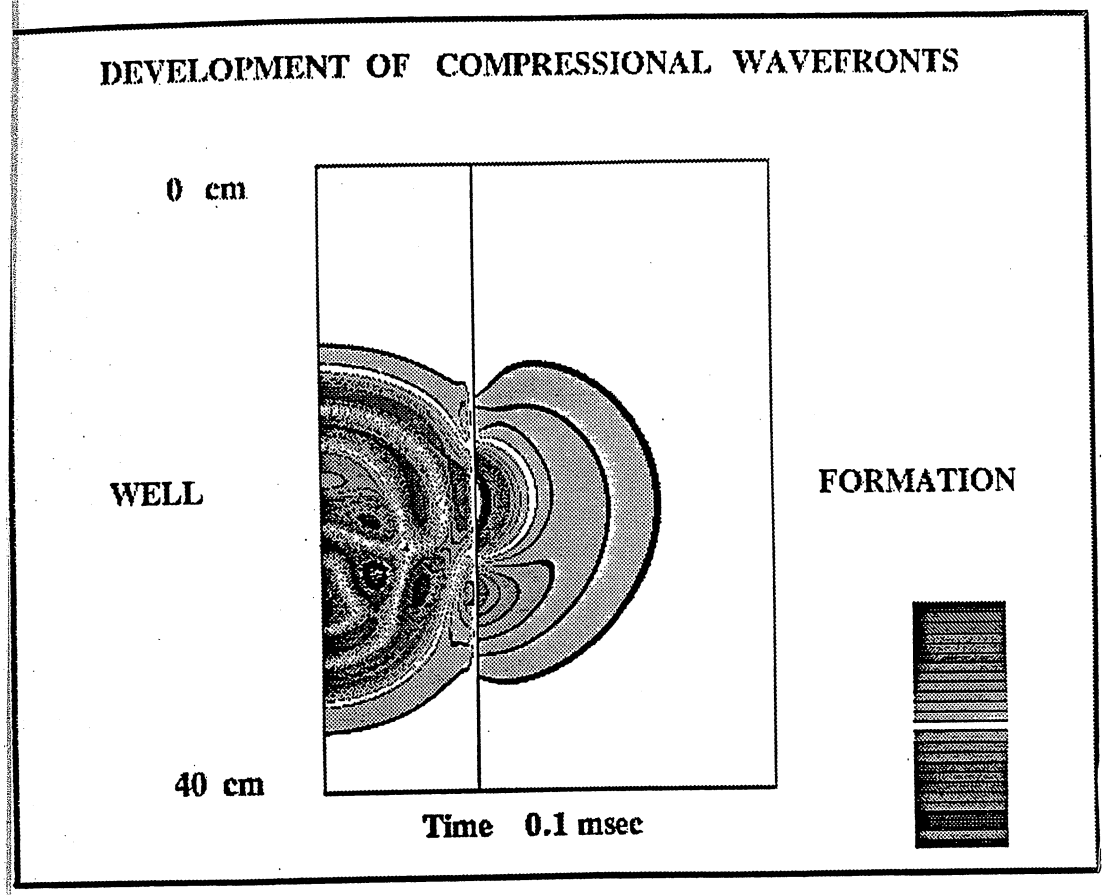

2 21 khz sources; lower source delayed

Figure 3

WELL–LOGGING EXAMPLE

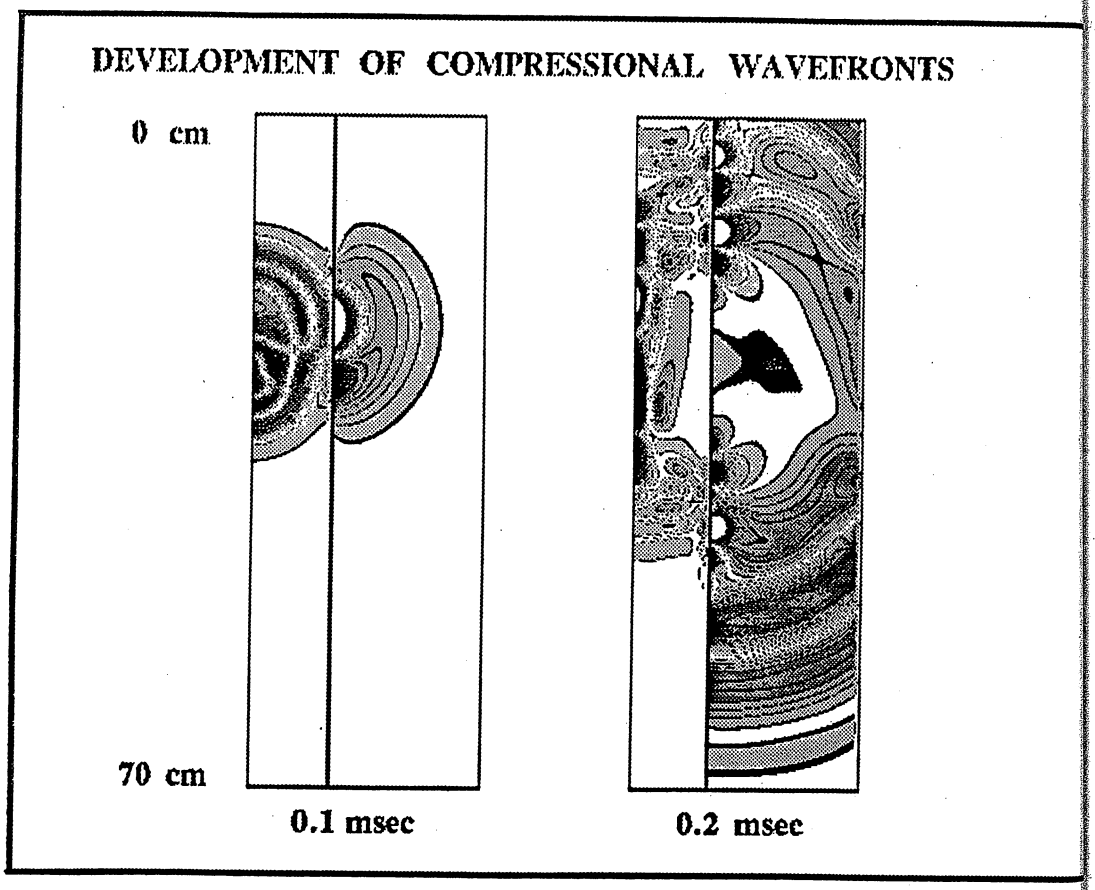

2 21 khz sources; lower source delayed

Figure 4

The same effects
where we show snapshot
in the well and the total
$u_{2z} + u_{3z}$) also at times
wavefronts in the forma
too early to see a separa
speeds.

In Figure 6 we sh
borehole and for the wa
each geophone are mark
travelling downward thr
$p1^*$ and $p1^{**}$ correspon
wave.

Figure 7 shows tl
depth 240 cm in the bo
the type I compression
ple reflections $p1^*$ an
sponds to the arrival c
wave generated by ener
gle $\theta_{sh} = \sin^{-1}\left(\frac{\text{boreh}}{\text{sl}}\right.$
the borehole and travel
Its arrival time can be
surface-related wave, tl
velocity smaller than tl
is the packet arriving a

To compare the
rant fluids and their efl
water-saturated Berea
sandstone. The gas and

In Figure 8 we pl
cm for both the gas –
smaller amplitude is ob
is explained by the fact
the pores is much stror
saturated sandstone, d
the gas. Also, the arriv
gas-saturated formatio
of the water-saturated

The same effects as in Figures 3 and 4 are appreciated in Figure 5, where we show snapshots for the displacement in the z-direction in the fluid in the well and the total displacement in the z-direction in the formation (i.e., $u_{2z} + u_{3z}$) also at times .1 msec and .2 msec. The compressional and shear wavefronts in the formation cannot be distinguished in Figure 5 because it is too early to see a separation between them as a consequence of their different speeds.

In Figure 6 we show the recorded pressure traces at the center of the borehole and for the water-saturated Berea sandstone. The arrival times at each geophone are marked for the type I and shear waves and the direct wave travelling downward through the fluid in the well, as well as the arrival times $p1^*$ and $p1^{**}$ corresponding to multiple reflections of the type I compressional wave.

Figure 7 shows the pressure trace recorded at the receiver located at depth 240 cm in the borehole. Again, we have marked the arrival times for the type I compressional waves, shear waves, direct waves, and the multiple reflections $p1^*$ and $p1^{**}$. The strong arrival at time 1.4 msec corresponds to the arrival of the so-called pseudo-Raleigh wave [14]. This is a wave generated by energy hitting Γ_3 at angles greater than the critical angle $\theta_{sh} = \sin^{-1}\left(\frac{\text{borehole fluid velocity}}{\text{shear velocity}}\right)$. Such energy is reflected back in the borehole and travels downward without leaking energy in the formation. Its arrival time can be estimated from phase velocity tables in [14]. Another surface-related wave, the Stoneley wave, travels with a frequency dependent velocity smaller than the fluid velocity v_f in the borehole. Thus, this wave is the packet arriving after the direct wave.

To compare the results of a well-logging test for two different saturant fluids and their effect in the recorded traces, we show the results of the water-saturated Berea sandstone with the corresponding gas-saturated Berea sandstone. The gas and water properties are given in Table 1.

In Figure 8 we plot the pressure recorded at the reveiver at depth 240 cm for both the gas – and water – saturated Berea sandstone, and a much smaller amplitude is observed for the water trace than for the gas trace. This is explained by the fact that the dissipative effects of the relative flow inside the pores is much stronger in the water-saturated sandstone than in the gas-saturated sandstone, due to the higher viscosity of the water with respect to the gas. Also, the arrival times of the different waves are slightly later for the gas-saturated formation due to its lower bulk modulus as compared to that of the water-saturated formation. Similar effect can be observed in Figures 9

and 10, where we have plotted the total displacement in the r-direction (i.e., $u_{2r} + u_{3r}$) and the trace of the total stress in the formation as functions of time.

WELL–LOGGING EXAMPLE

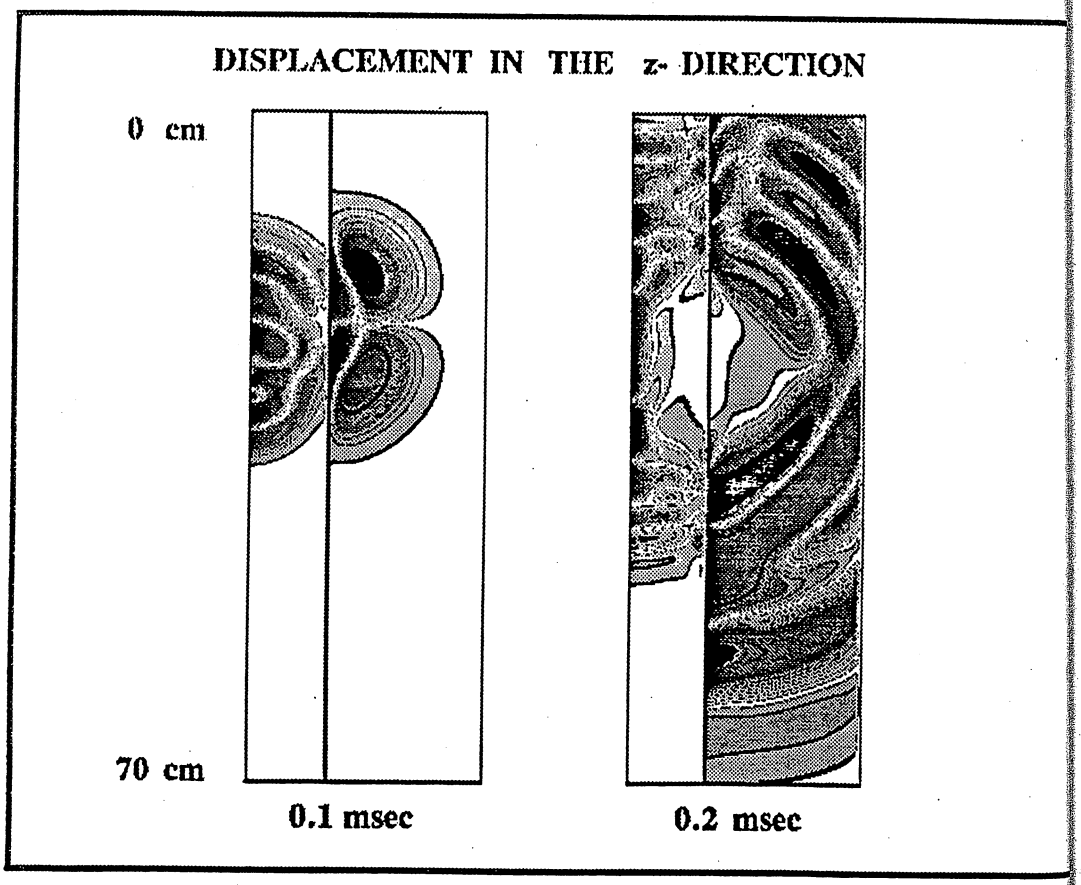

2 21 khz sources; lower source delayed

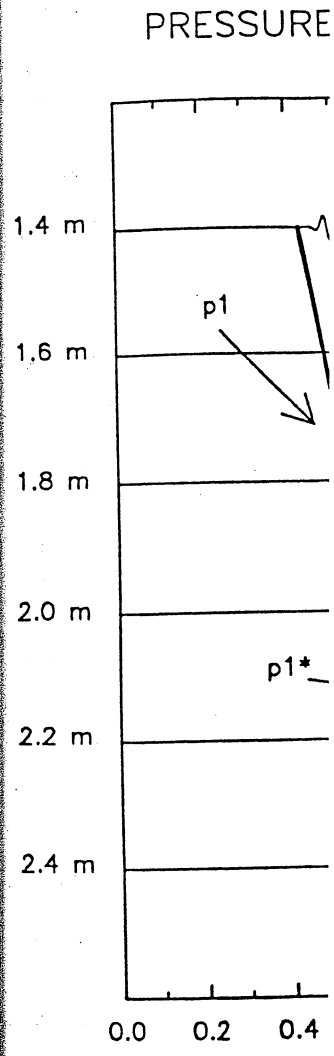

Figure 5

nent in the r-direction (i.e.,
e formation as functions of

.MPLE

)IRECTION

2 msec

:e delayed

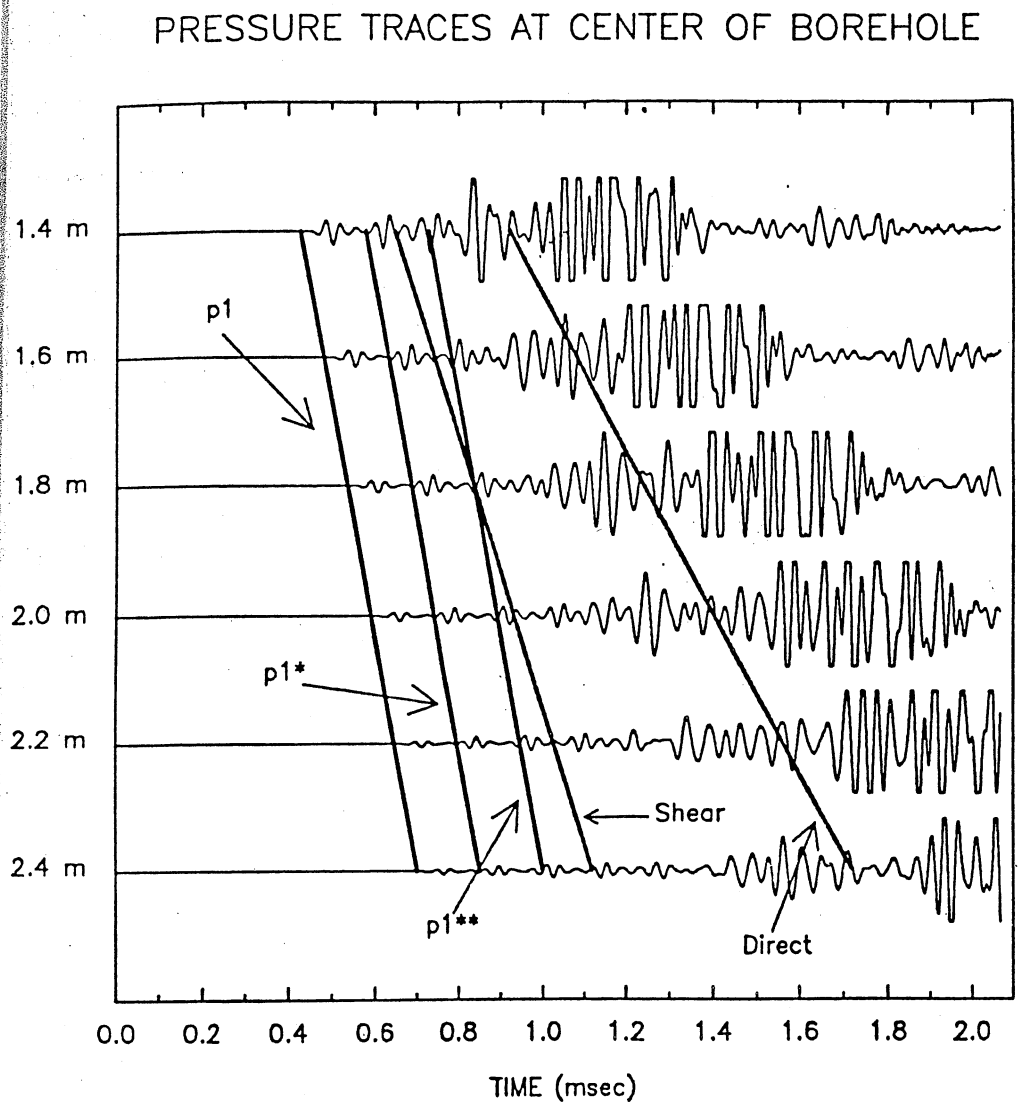

Figure 6

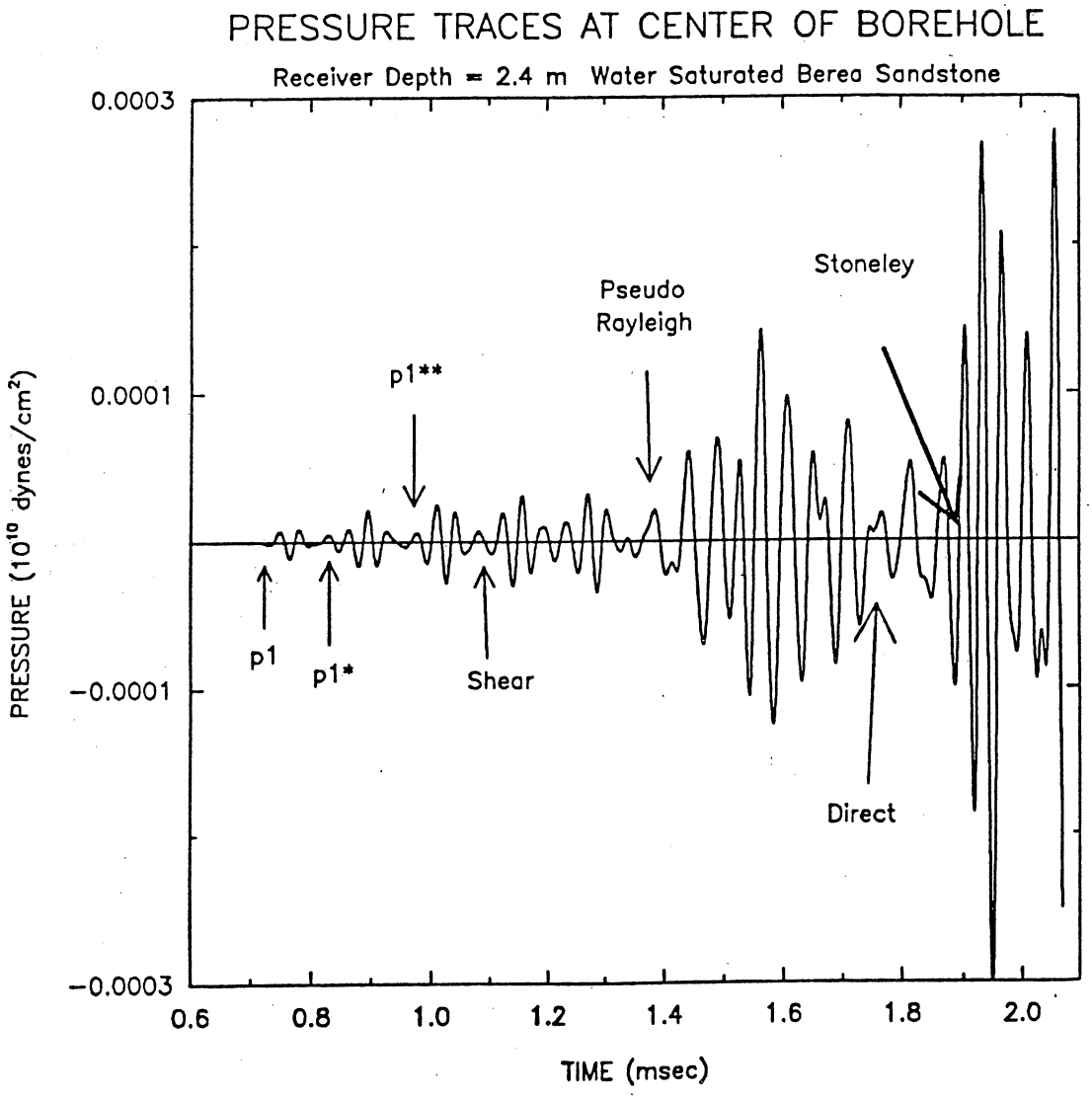
PRESSURE TRACES AT CENTER OF BOREHOLE
Receiver Depth = 2.4 m Water Saturated Berea Sandstone
PRESSURE (10^10 dynes/cm^2)
0.0003
0.0001
−0.0001
−0.0003
0.6
0.8
1.0
1.2
1.4
1.6
1.8
2.0
TIME (msec)
p1
p1*
p1**
Shear
Pseudo Rayleigh
Stoneley
Direct

Figure 7

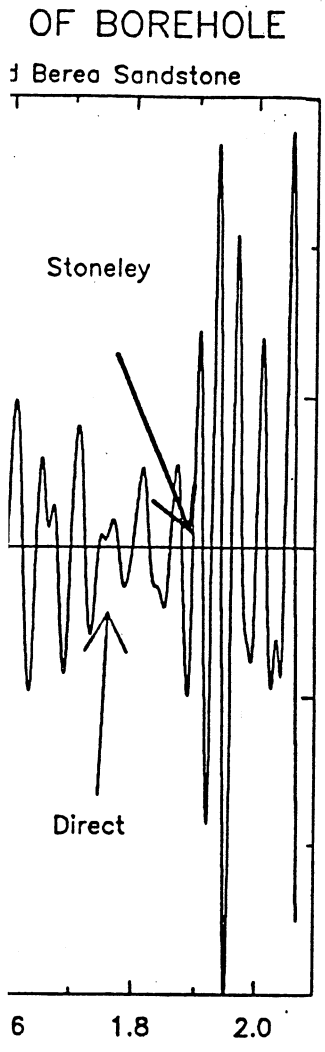
OF BOREHOLE
d Berea Sandstone
Stoneley
Direct
6
1.8
2.0

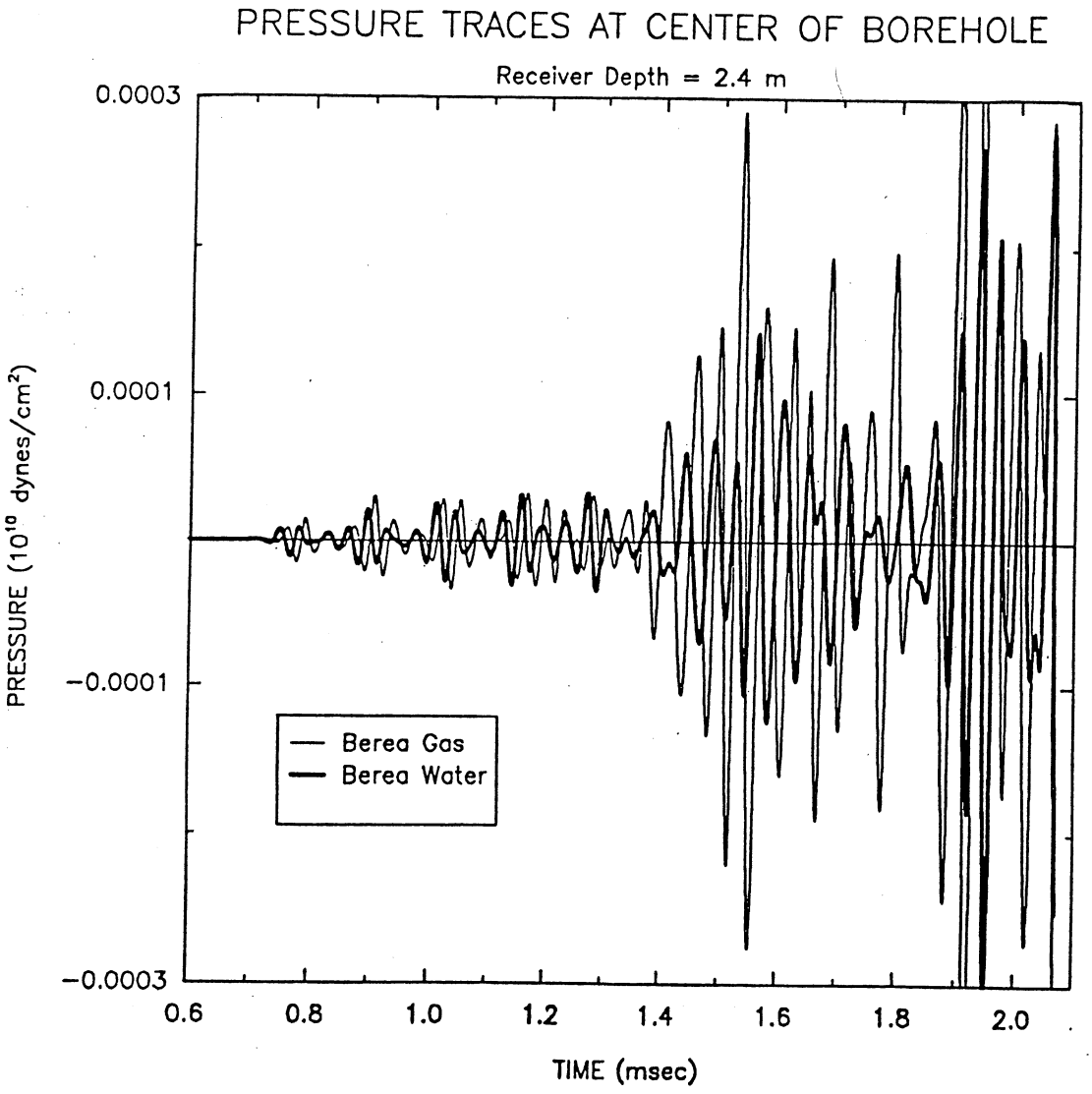
PRESSURE TRACES AT CENTER OF BOREHOLE
Receiver Depth = 2.4 m
0.0003
0.0001
−0.0001
−0.0003
PRESSURE (10¹⁰ dynes/cm²)
Berea Gas
Berea Water
0.6
0.8
1.0
1.2
1.4
1.6
1.8
2.0
TIME (msec)

Figure 8

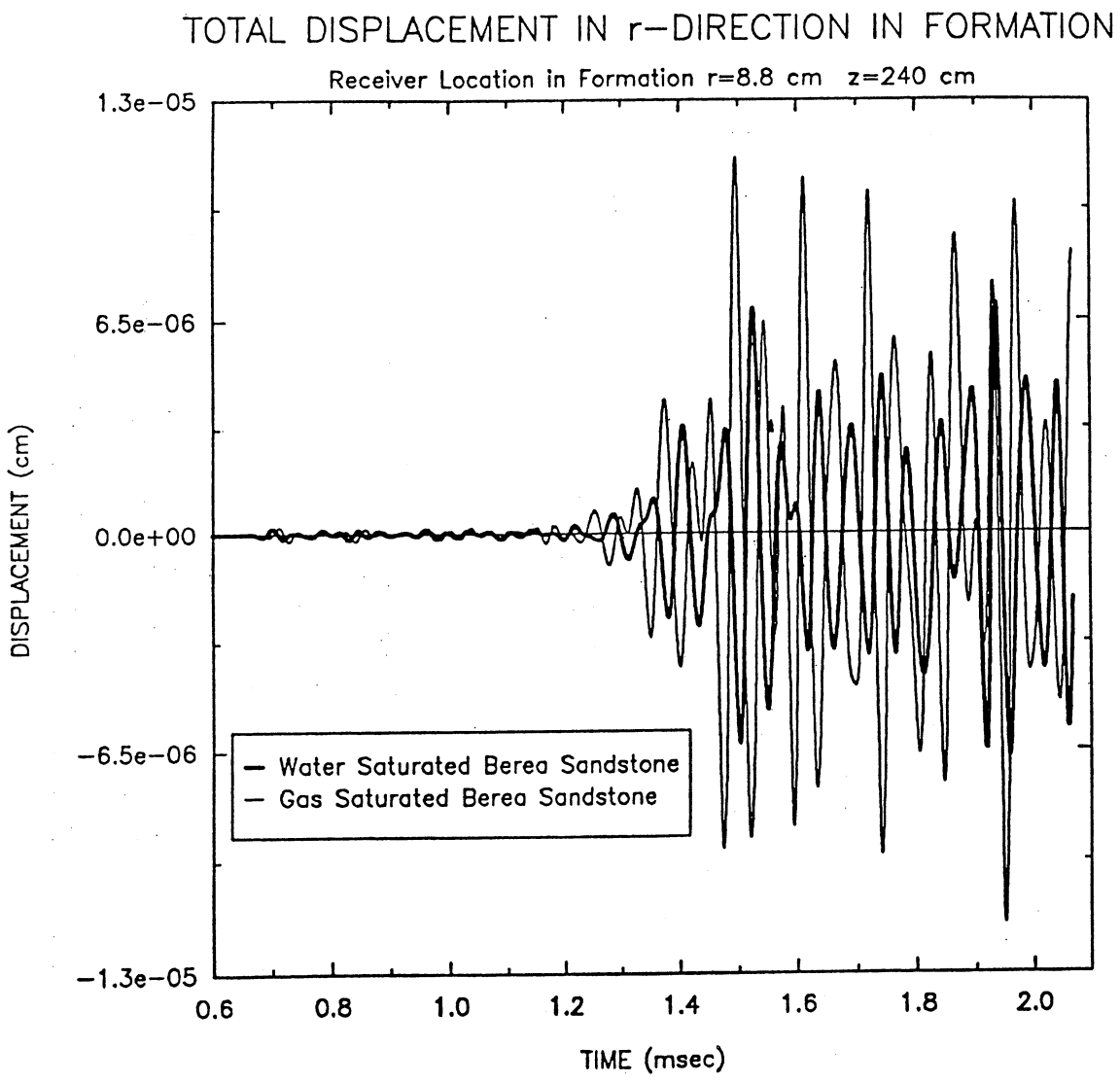
TOTAL DISPLACEMENT IN r–DIRECTION IN FORMATION
Receiver Location in Formation r=8.8 cm z=240 cm
1.3e-05
6.5e-06
0.0e+00
-6.5e-06
-1.3e-05
DISPLACEMENT (cm)
0.6
0.8
1.0
1.2
1.4
1.6
1.8
2.0
TIME (msec)
— Water Saturated Berea Sandstone
— Gas Saturated Berea Sandstone

Figure 9

N IN FORMATION

z=240 cm

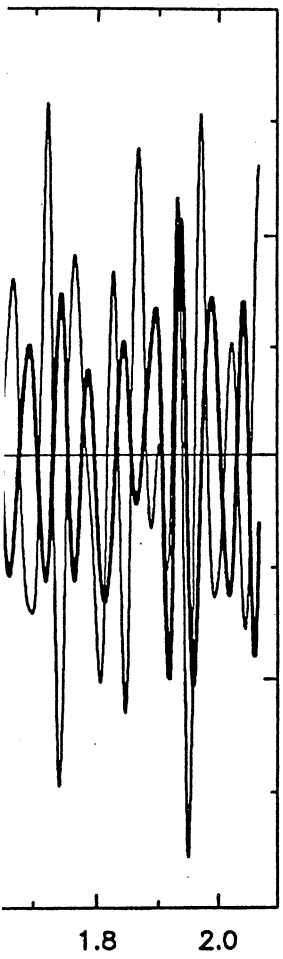

TRACE OF TOTAL STRESS IN FORMATION

Receiver Location in Formation r=8.8 cm z=240 cm

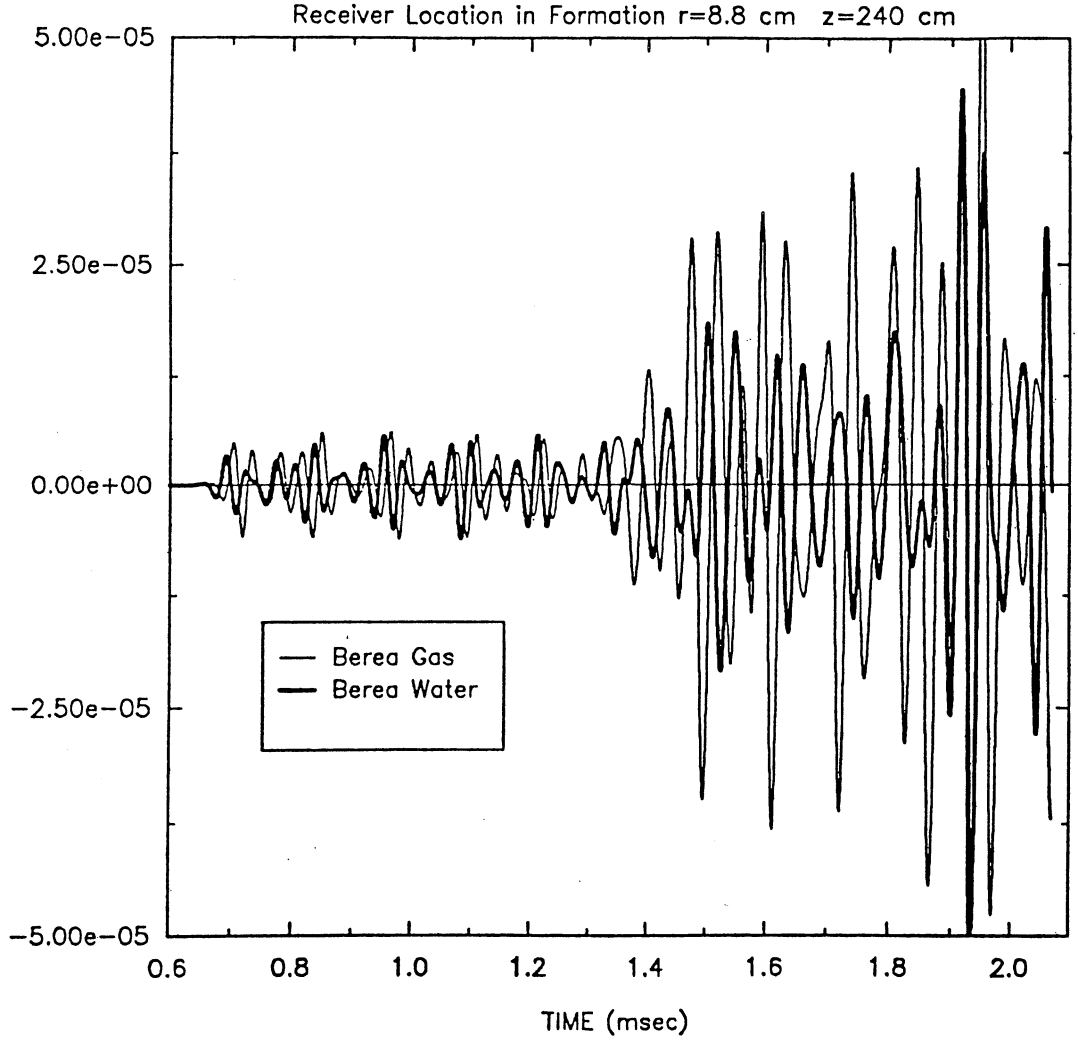

Figure 10

TABLE 1

	Water Saturated Berea	Gas Saturated Berea
A	$12.3170 \frac{10^{10} \text{ dynes}}{\text{cm}^2}$	$8.7051 \frac{10^{10} \text{ dynes}}{\text{cm}^2}$
N	$10.1542 \frac{10^{10} \text{ dynes}}{\text{cm}^2}$	$10.1542 \frac{10^{10} \text{ dynes}}{\text{cm}^2}$
Q	$6.2493 \frac{10^{10} \text{ dynes}}{\text{cm}^2}$	$.1728 \frac{10^{10} \text{ dynes}}{\text{cm}^2}$
H	$10.5136 \frac{10^{10} \text{ dynes}}{\text{cm}^2}$	$.2908 \frac{10^{10} \text{ dynes}}{\text{cm}^2}$
ρ	2.3365 g/cm^3	2.1731 g/cm^3
ρ_f	1 g/cm^3	.1398 g/cm^3
ϕ	.19	.19
K	200 md	200 md
μ	1.00 cp	.022 cp
g	14.73 g/cm^3	2.06 g/cm^3
ρ_s	2.65 g/cm^3	2.65 g/cm^3

More numerical experiments are needed to show the effects of variable in-depth borehole diameter, inhomogenities, mud-cake, and permeability on the recorded traces.

Also, the inclusion of frequency dependent permeabilities following the homogenization procedure in [1], [4] to modity Biot's equation would eventually lead to more accurate synthetic seismograms.

[1] J.L. Auriault, G
flowing through
pp. 105-128.

[2] M.A. Biot, *Thec*
solid. I. Low fre

[3] — , *Mechanics c*
Applied Physics,

[4] R. Burridge and
ture, J. Acoust.

[5] N.C. Dutta and
sics, 48 (1983), p

[6] Y.C. Fung, *Four*

[7] A.E. Love, *A T*
University Press

[8] O.M. Lovera, *Bo*
52 (1987), pp. 1

[9] M.E. Morley, *Ve*

[10] R.W. Morse, *Ac*
(1952), pp. 696-

[11] J.H. Rosenbaum
Geophysics, 39 (

[12] J.E. Santos, J.
methods for a m
8 (1988), pp. 41

[13] R.A. Stephen, F.
stic logs, Geophy

[14] J. Tittman, *Geo*

Jim DOUGLAS, Jr. -
Juan E. SANTOS - Y
Jeffrey L. HENSLEY
Mary E. MORLEY -

REFERENCES

[1] J.L. Auriault, G. Bonnet and O. Lebaigue, *Dynamics of two immiscible fluid flowing through deformable porous media*, Transport in Porous Media, 4 (1989), pp. 105-128.

[2] M.A. Biot, *Theory of propagation of elastic waves in a fluid-saturated porous solid. I. Low frequency range*, J. Acoust. Soc. Am., 28 (1956), pp. 168-178.

[3] — , *Mechanics of deformation and acoustic propagation in porous media*, J. of Applied Physics, 33 (1962), pp. 1482-1498.

[4] R. Burridge and J.B. Keller, *Poroelasticity equations derived from microstructure*, J. Acoust. Soc. Am., 70 (1981), pp. 1140-1145.

[5] N.C. Dutta and H. Odé, *Seismic reflections from a gas-water contact*, Geophysics, 48 (1983), pp. 148-162.

[6] Y.C. Fung, *Foundations of Solid Mechanics*, Prentice Hall, 1965.

[7] A.E. Love, *A Treatise on the Mathematical Theory of Elasticity*, Cambridge University Press, fourth edition, London, 1927.

[8] O.M. Lovera, *Boundary conditions for a fluid-saturated porous solid*, Geophysics, 52 (1987), pp. 174-178.

[9] M.E. Morley, *Vector finite elements for radially symmetric problems*, to appear.

[10] R.W. Morse, *Acoustic propagation in granular media*, J. Acoust. Soc. Am., 24 (1952), pp. 696-700.

[11] J.H. Rosenbaum, *Synthetic microseismograms: Logging in porous formations*, Geophysics, 39 (1974), pp. 14-32.

[12] J.E. Santos, J. Douglas, Jr., M.E. Morley and O.M. Lovera, *Finite element methods for a model for full waveform acoustic logging*, IMA J. Numer. Anal., 8 (1988), pp. 415-433.

[13] R.A. Stephen, F. Cardo-Casas and C.H. Cheng, *Finite-difference synthetic acoustic logs*, Geophysics, 50 (1985), pp. 1588-1609.

[14] J. Tittman, *Geophysical Well Logging*, Academic Press, 1986.

Jim DOUGLAS, Jr. - Purdue University - U.S.A.

Juan E. SANTOS - Yacimientos Petrolíferos Fiscales and Purdue University - U.S.A.

Jeffrey L. HENSLEY - Purdue University - U.S.A.

Mary E. MORLEY - Temple University - U.S.A.